Mineralogical Magazine (2023), **87**, 702–710
doi:10.1180/mgm.2023.68

CAMBRIDGE UNIVERSITY PRESS

Article

Ferric iron in chrome-bearing spinels: implications for microprobe correction procedures

Hugh Rollinson and Jacob Adetunji
School of Built and Natural Environment, University of Derby, Kedleston Road, Derby, DE22 1GB, UK

Abstract

We investigated the compositions of a suite of 361 chrome-bearing spinels from spinel peridotites, ophiolitic mantle chromitites and from layered igneous intrusions in which the Fe^{2+}/Fe^{3+} ratio has been determined by Mössbauer spectroscopy. We explore the crystal-chemical controls on the distribution of Fe^{3+} and on mineral stoichiometry with regard to electron-probe correction procedures for estimating Fe^{3+} in spinel. We find that chrome-bearing spinels can be subdivided into three groups: a Cr–Al-rich group; a high-Fe group; and a highly oxidised group. Spinels of the Cr–Al group are found in spinel peridotites and ophiolitic mantle chromitites. They are normal spinels with a low Fe^{3+} content and compositions that are close to stoichiometric. Spinels in the high-Fe group are found in layered igneous intrusions. They are also normal spinels which have higher concentrations of Fe^{3+} on the octahedrally coordinated site than is found for the Cr–Al group. Stoichiometric calculations tend to overestimate the Fe^{3+} content and their compositions do not conform to the MgO–cr# correlation found in the Cr–Al group. Spinels in the highly oxidised group are found in layered intrusions and ophiolitic mantle chromitites. They have $(Fe^{3+}/\Sigma Fe)_{Möss} > 0.4$ and high Cr (cr# > 0.5), but relatively low Fe^{2+} (fe# 0.24–0.56). Stoichiometric calculations tend to underestimate the Fe^{3+} content. They represent normal spinels in which tetrahedrally coordinated Fe^{2+} has been oxidised to Fe^{3+}.

Our data show that spinels with greater Cr and Fe are sufficiently different in their crystal chemistry from the aluminous spinels to indicate that the EPMA correction procedures developed for Fe^{3+} in aluminous spinels on the basis of the Cr/Al ratio, and used in oxy-thermobarometry, are inappropriate for Cr-rich and Fe-rich compositions.

Keywords: ferric iron; spinel; chromite; stoichiometry; Mössbauer spectroscopy; electron-probe micro-analysis; EPMA

(Received 12 June 2023; accepted 11 August 2023; Accepted Manuscript published online: 12 September 2023; Associate Editor: Ferdinando Bosi)

Introduction

The ferrous/ferric iron ratio in spinels is an important source of information in calculating the oxidation state of the Earth's mantle and derivative melts. This is particularly important in the application of oxy-thermobarometers such as those based on olivine–orthopyroxene–spinel equilibria (Wood and Virgo, 1989; Wood, 1990; Ballhaus *et al.*, 1991; Davis *et al.*, 2017; Stagno and Fei, 2020). Stagno (2019) used this method to show a correlation between the $Fe^{3+}/\Sigma Fe$ ratio in Cr-bearing spinels from mantle spinel peridotites and the oxygen fugacity ($\log f_{O_2}$) of the upper mantle demonstrating that the $Fe^{3+}/\Sigma Fe$ ratio in Cr-bearing spinels is an important proxy for mantle f_{O_2}.

However, for this application to be a success it is essential to have an accurate knowledge of the relative abundances of Fe^{2+} and Fe^{3+} in spinel, and as yet estimating Fe^{3+} abundances in chrome spinels is not straightforward. Here we investigate the compositions of natural chrome-bearing spinels in which the bulk compositions were determined using electron probe microanalysis (EPMA) and the Fe^{2+}/Fe^{3+} ratio measured directly using Mössbauer spectroscopy. Using this dataset, we explore the distribution of Fe^{3+} over a wide range of spinel compositions. This work is based on our earlier studies of chromite in chromitites from the mantle section of the Oman ophiolite and from layered mafic igneous intrusions. In addition, we have incorporated data from other published studies which have combined EPMA and Mössbauer data for chrome-bearing spinels. These investigations are principally of spinel-peridotites found either as xenoliths in basalt or preserved as orogenic massifs. A list of the data sources used is given in Supplementary Table S1.

Previous investigations by Wood and Virgo (1989), Dare *et al.* (2009) and Davis *et al.* (2017) measured Fe^{3+} in spinels by EPMA using a set of secondary microprobe standards in which Fe^{3+} had been determined by Mössbauer spectroscopy. They found a correlation between the offset between $(Fe^{3+}/\Sigma Fe)_{Möss}$ and $(Fe^{3+}/\Sigma Fe)_{EPMA}$ [represented by $(\Delta Fe^{3+}/\Sigma Fe)_{Möss\text{-}EPMA}$] and cr#. They used this correlation to correct the $Fe^{3+}/\Sigma Fe$ values calculated from EPMA/stoichiometric constraints. Davis *et al.* (2017) noted that although this correction works well for aluminous spinels in lherzolites, the subject of the Wood and Virgo (1989) study, and that it might not work so well for compositions beyond this range. Here we use an expanded database which includes Cr-rich and Fe-rich compositions and from which we confirm the concerns of Davis *et al.* (2017) regarding the EPMA

Corresponding author: Hugh Rollinson; **Email:** h.rollinson@derby.ac.uk
Cite this article: Rollinson H. and Adetunji J. (2023) Ferric iron in chrome-bearing spinels: implications for microprobe correction procedures. *Mineralogical Magazine* **87**, 702–710. https://doi.org/10.1180/mgm.2023.68

correction procedure. We show that Cr- and Fe-rich spinels exhibit different crystal chemical features from the aluminous spinels providing new insights into the distribution of Fe^{3+} in spinels. These observations imply that the correction procedures developed for aluminous spinels are inappropriate for Cr-rich and Fe-rich compositions.

Spinel structure

Minerals of the spinel group conform to a near-ideal cubic structure of close-packed oxygen atoms. There are 32 oxygen atoms in the unit cell between which there are tetrahedrally and octahedrally coordinated cation sites. Of the 24 cation sites, 8 are tetrahedrally coordinated and designated *T* sites which accommodate cations of the A atom group and 16 are octahedrally coordinated and designated *M* sites that accommodate cations of the B atom group (Bosi *et al.*, 2019). Following O'Neill and Navrotsky (1983) the spinels under consideration here are 2–3 spinels, i.e. cations of the A atom group have a 2^+ charge and include Mg, Fe^{2+}, Zn and Mn, and cations of the B atom group have a 3^+ charge and include Al, Fe^{3+} and Cr. Using the unit cell model adopted here normal spinels have the structure $(A)_8[B_{16}]O_{32}$ in which the divalent A cations occupy the tetrahedrally coordinated sites and the trivalent B cations the octahedrally coordinated sites; they include phases such as $MgAl_2O_4$ (spinel proper) and $FeCr_2O_4$ (chromite). Inverse spinels have the structure $(B)_8[A,B]_{16}O_{32}$ and include minerals such as $(Fe^{3+})[Fe^{2+}Fe^{3+}]O_4$ (magnetite).

However, the crystal chemistry of spinels, in particular their cation distribution, is not straightforward. For example, as many authors have shown (Dyar *et al.*, 1989; Canil *et al.*, 1990; Davis *et al.*, 2017) chrome-spinels are commonly non-stoichiometric and could therefore contain vacancies at cation sites, contain cations at interstitial sites, or be oxygen deficient (Fregola *et al.*, 2011). Furthermore, spinels can display complex disordering between the two cation sites and show a full range of cation distributions between the normal and inverse spinel structures. This could be quantified by the parameter *x*, which is the fraction of tetrahedrally coordinated sites occupied by B cations. Because ions on the *T* and *M* sites have different sizes, a change in *x* results in a change in the dimensions of the unit cell (O'Neill and Navrotsky, 1983). Experimental investigations by Nell and Wood (1989, 1991) and Nell *et al.* (1989) show that in the spinel system $(Mg^{2+}, Fe^{2+})(Fe^{3+}, Al^{3+}, Cr^{3+})_2O_4$ under consideration here, there is Fe^{2+}, Mg^{2+}, Fe^{3+} and Al^{3+} disorder between tetrahedrally and octahedrally coordinated sites. In contrast, Cr^{3+} is present only at octahedrally coordinated sites because of its size and high crystal field stabilisation energy, and there is no observed cation disordering in the system $FeCr_2O_4$–$MgCr_2O_4$ (Nell and Wood, 1991). These observations imply that in natural spinels it is commonly difficult to assign precisely cations to their appropriate crystallographic site. Full details of site occupancies can be obtained from single-crystal X-ray diffraction data using a fitting model in which the atomic fractions at the two sites are calculated. Some insight can also be gained from Mössbauer spectroscopy for the site occupancy of Fe^{2+} and Fe^{3+} ions (Schmidbauer, 1987; Rollinson *et al.*, 2012).

Methodology

This investigation is based on a data set of samples analysed in our laboratory, augmented by an extended dataset of previously published data. All data have been processed in the same manner using EPMA data and Fe^{2+}/Fe^{3+} ratios determined by Mössbauer spectroscopy. We have not assumed that our spinels are stoichiometric. For this reason our cation calculations are based upon 32 oxygens (the number of oxygen ions in the unit cell) to give an expected composition $[A^{2+}]_8[B^{3+}]_{16}O_{32}$. This leaves the cation totals to vary around the value of 24.0. Totals that deviate significantly from this value, after allowing for small errors in the microprobe analysis, might indicate non-stoichiometry. Details of the samples used and the compositional data are given in Supplementary Tables S1–S3.

Full details of the methodological approaches that lie behind this investigation – Mössbauer analysis, EPMA, the cation calculation scheme and site-occupancy calculations are given in the Supplementary Material. This discussion includes a full consideration of the systematic errors in the different methodologies employed in our core data set. These data are then used to set limits on the systematic errors in our extended dataset. Representative Mossbauer fitting parameters are given in Supplementary Table S4.

In the text below we use the terms: 'chrome-bearing spinel' to include: the spinel–magnesio-chromite series and the magnesio-chromite–chromite series; and 'uncorrected EPMA' (electron probe microanalysis) for data where Fe^{3+} (if calculated) is based on the assumption of ideal stoichiometry (24 cations per 32 oxygens), although without a correction based on Mössbauer-calibrated spinels, as described, for example, by Wood and Virgo (1989) and Davis *et al.* (2017).

Results

A plot of samples by provenance is shown in Fig. 1 on a cr# (Cr/(Cr+Al) vs. fe# (Fe^{2+}/(Fe^{2+}+Mg) diagram. Spinels in the peridotite xenoliths range in cr# from 0.016–0.862 and in the spinel peridotite massifs from 0.046–0.436; spinels from the peridotite massifs are slightly more Fe-rich than those in the xenoliths. A subset of samples from metasomatised mantle xenoliths containing aluminous phases are more Cr-rich than samples which are not metasomatised. Spinels in these series show a small increase in fe# with increasing cr#. Spinels in mantle chromitites from ophiolite complexes are Cr-rich and show a wide range of compositions (cr# = 0.286–0.845, fe# = 0.0–0.563). Most spinels in this series show an increase in cr# with no associated increase in fe#. Spinels from layered mafic intrusions are more Fe-rich and vary with cr# = 0.490–0.845 and fe# = 0.278–0.838, and show a broad trend of decreasing cr# with increasing fe#. In total our data set comprises 361 Mössbauer measurements of Fe^{2+}/Fe^{3+} in Cr-bearing spinels; compositions range from cr# = 0.016–0.862 and fe# = 0.0–0.838, i.e. from spinel to magnesio-chromite and chromite. We measured $Fe^{3+}/\Sigma Fe$ ratios between 0.05 and 1.0 and low Ti concentrations between 0.002–0.286 apfu (atoms per formula unit), with a mean = 0.038 apfu.

Cation plots

Crystal-chemical data shown as cation plots suggest that the chrome-bearing spinels examined in this investigation fall into three distinct groups. All the plots described below show cations from the corrected EPMA, that is, the cations are recalculated using Fe^{3+} from Mössbauer data.

https://doi.org/10.1180/mgm.2023.68 Published online by Cambridge University Press

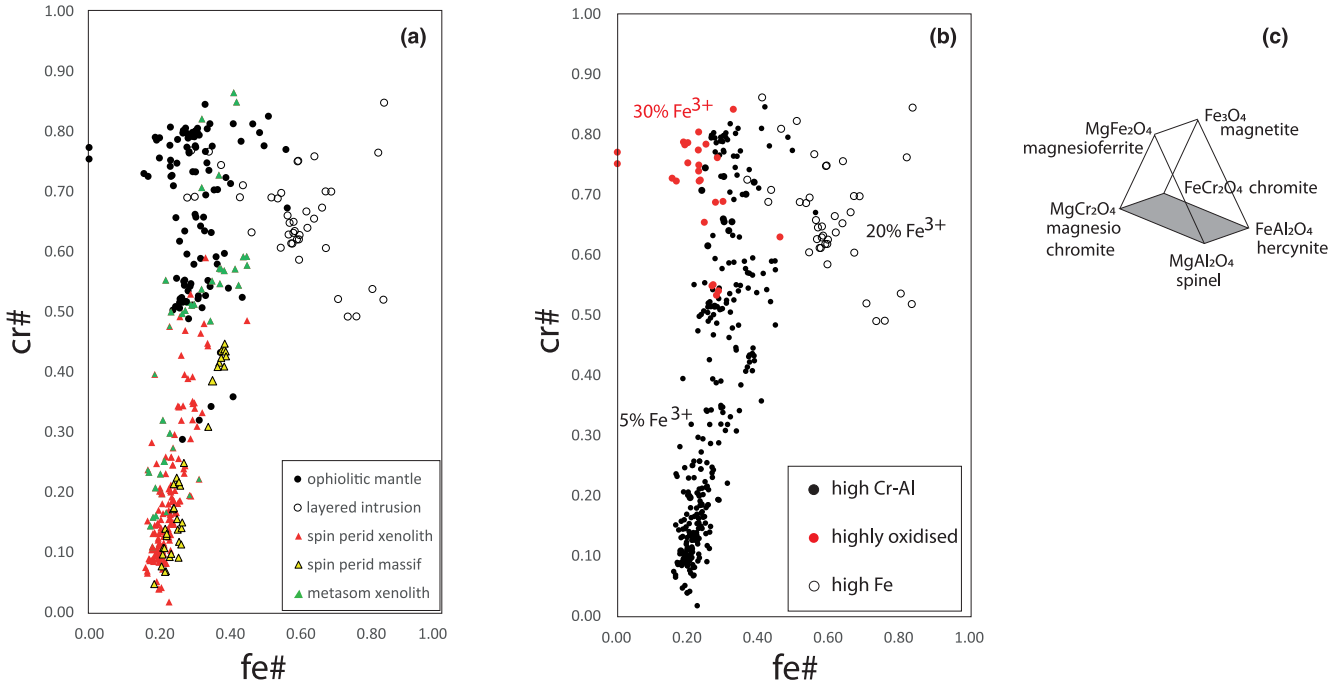

Figure 1. (a) Plot of cr# vs. fe# by provenance for the samples used in this study; (b) plot of cr# vs. fe# showing the three main groups of samples identified in this study. The proportion of Fe^{3+} cations expressed as $Fe^{3+}/(Fe^{3+}+Al+Cr)$ is also shown; (c) the location of the cr# vs. fe# plot is shown as the grey area within the spinel prism of Haggerty (1991). Samples with a high magnesioferrite-magnetite content are projected onto the base of this prism. In diagrams (a) and (b) cr# and fe# are corrected using the Mössbauer $Fe^{3+}/\Sigma Fe$, as described in the text.

Group 1 – highly oxidised spinels

A plot of $(Fe^{3+}/\Sigma Fe)_{Möss}$ vs. cr# for all spinels shows that some samples have anomalously high $(Fe^{3+}/\Sigma Fe)_{Möss}$ ratios (Fig. 2). Here we define anomalously high as $(Fe^{3+}/\Sigma Fe)_{Möss} > 0.4$; this is consistent with samples that have ratios higher than 2σ above the data trendline on a $(Fe^{3+}/\Sigma Fe)_{Möss}$ vs. cr# plot (Fig. 2) and is consistent with the most highly oxidised Cr-bearing spinels found in the natural spinel peridotites described in the review by Stagno (2019).

These samples define a group of highly oxidised chrome-rich spinels. They are shown in red in Fig. 2. They have high $Fe^{3+}/(Fe^{3+}+Al+Cr)$ ratios in the range 0.16–0.46 (mean = 0.288). Their position in Fig. 1b therefore represents a projection from magnesioferrite–magnetite join onto the base of the spinel prism of Haggerty (1991). Samples in this group come from ophiolitic mantle chromitites and chromitites in layered intrusions.

Group 2 – Cr–Al spinels

When the highly oxidised samples identified above are removed from the dataset, a plot of Cr vs. Al apfu shows two populations (Fig 3a). Samples with (Cr+Al) between 16.0 and 14.83 follow an inverse straight-line relationship ($R^2 = 0.997$), close to the stoichiometric 16 cation line for octahedrally coordinated cations in normal spinels and apparently indicating an almost exclusive Cr–Al substitution. These samples have low $Fe^{3+}/(Fe^{3+} + Al + Cr)$ ratios in the range 0.007–0.18 (mean = 0.055). Most samples in this group are either from spinel peridotites or ophiolitic mantle chromitites.

Group 3 – high-Fe spinels

A second group of samples on a Cr vs. Al cation plot diverges from the straight-line trend noted above at about Al = 8.0 apfu, with Cr values lower than those observed in the Cr–Al group. These samples have Cr + Al = 14.83–11.49. They are further characterised by their high total Fe content and $Fe^{2+} + Fe^{3+} > 4.2$ apfu (Fig 3b). This distinction is also apparent on the cr# vs. fe# plot indicating that these samples have high $Fe^{2+}/(Fe^{2+}+Mg)$ ratios (Fig. 1b). Previous studies have also recognised this distinction on the basis of single-crystal X-ray data (Lenaz *et al.*, 2011; Velicogna and Lenaz, 2017; Menagazzo *et al.*, 1997) and using a combination of single-crystal X-ray data and Mössbauer data (Bosi *et al.*, 2004; Figueiras and Waerenborgh, 1997). A comparison between Figs 1a, 1b and 3b shows that these high-Fe samples are from layered igneous intrusions. These samples have $Fe^{3+}/(Fe^{3+}+Al+Cr)$ ratios in the range 0.011–0.53 (mean = 0.20). A further distinction between the two groups is seen in the MgO vs. cr# plot (Fig. 3c) where the Cr–Al spinels plot with a negative trend whereas the high-Fe spinels plot with a positive trend and with lower MgO values (cf. Davis *et al.* (2017).

Stoichiometry

Mössbauer spectroscopy is the only direct means of accurately measuring Fe^{3+} in spinels, therefore our data can be used to evaluate the reliability of Fe^{3+} calculated assuming mineral stoichiometry and thereby assess the degree to which spinels are stoichiometric. Previous Mössbauer studies of Fe^{3+} in spinel peridotites have shown that there is a discrepancy between Fe^{3+} calculated from uncorrected EPMA assuming perfect stoichiometry and that measured by Mössbauer spectroscopy (Dyar *et al.*, 1989; Canil *et al.*, 1990; Davis *et al.*, 2017). Here we extend this conclusion to the Cr-rich and Fe-rich spinels described in this work.

A comparison of $(Fe^{3+}/\Sigma Fe)_{Möss}$ as measured by Mössbauer and $(Fe^{3+}/\Sigma Fe)_{stoich}$ calculated from uncorrected EPMA using

https://doi.org/10.1180/mgm.2023.68 Published online by Cambridge University Press

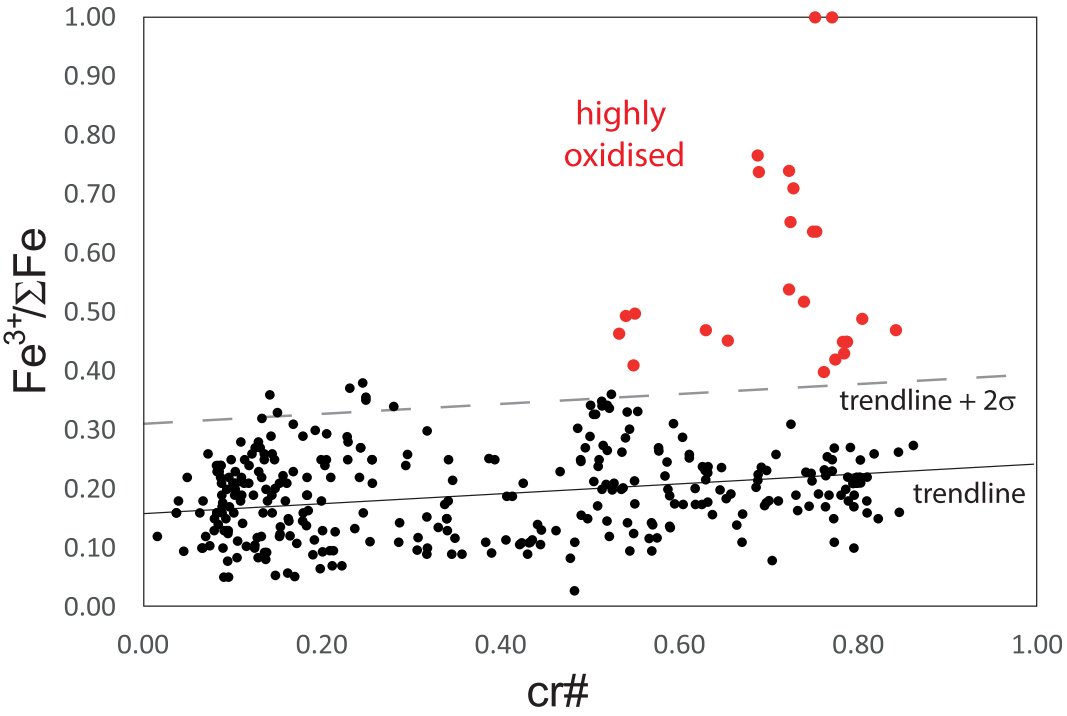

Figure 2. Plot of $Fe^{3+}/\Sigma Fe$ as determined by Mössbauer spectroscopy vs. cr#. Samples with anomalously high $Fe^{3+}/\Sigma Fe$, (i.e. $Fe^{3+}/\Sigma Fe > 0.4$) are shown in red and designated 'highly oxidised'. The geological settings of the two groups of samples are given in Fig. 1 (a and b).

the stoichiometric/charge-balance equation of Droop (1987) is shown in Fig. 4a. Many samples are not stoichiometric and there are differences between the different groups of spinels. The $Fe^{3+}/\Sigma Fe$ ratio of the highly oxidised spinels is significantly underestimated by stoichiometric calculations. This is also true for the Cr–Al group of spinels found in spinel peridotites and ophiolitic chromitites, which form a cloud of data points scattered around the 1:1 stoichiometric line, though with quite a high proportion of samples showing that stoichiometry underestimates the $Fe^{3+}/\Sigma Fe$ ratio. In contrast, many high-Fe samples plot below the 1:1 line indicating that stoichiometry overestimates the true $Fe^{3+}/\Sigma Fe$ ratio. A plot of the absolute values of Fe^{3+} in apfu is given in Fig. 4b, where $Fe^{3+}_{Möss}$ is plotted versus Fe^{3+}_{stoich} and shows the same pattern as in the $Fe^{3+}/\Sigma Fe$ ratio diagrams except that the groups are more clearly separated. A plot of Fe^{3+} versus the cation sum, from the cation calculation to 32 oxygens, shows the same three groups (Fig. 4c). Most of the Cr–Al samples have values close to 24.0 indicating that they approach stoichiometry. In contrast the Fe-rich and highly oxidised samples deviate from a cation total of 24.0. The highly oxidised samples have increasingly low cation totals as Fe^{3+} increases.

Discussion

Here we seek to interpret our observations of cation distributions in a subset of our Cr-bearing spinels with regard to site-occupancy calculations obtained from previous X-ray diffraction investigations. First, however, it is important to examine two processes that can alter the $Fe^{3+}/\Sigma Fe$ ratio in spinels in their post-magmatic state and thus have the potential to distort our observations.

Iron enrichment due to subsolidus Fe–Mg exchange occurs in rocks that have cooled slowly and where the chromite is disseminated in a silicate matrix. This is particularly true in dunitic rocks (see for example Rollinson and Adetunji, 2013; O'Driscoll *et al.*, 2021). Such a process will enhance the fe# and reduce the $Fe^{3+}/\Sigma Fe$ ratio to below the primary value, particularly in Fe-rich samples. This process could explain some of the low $(Fe^{3+}/\Sigma Fe)_{Möss}$ ratios in the Cr–Al group found in spinel peridotites and the scattered patterns in samples from ophiolitic mantle and from layered intrusions where the chromite is disseminated (Fig. 4a). However, most of the chromitites in the ophiolitic mantle and in layered intrusions occur as massive chromitites in which Fe–Mg exchange with a silicate phase is absent.

A second process, is metasomatic alteration of spinels by later melts and/or post-magmatic fluids. This was first proposed by Arai (1994) who showed that some spinel compositions can deviate from the olivine–spinel mantle array, either by interaction with alkaline-rich fluids or in cumulate rocks through fractionation. More recently El-Dien *et al.* (2019) has described a form of cryptic metasomatism where aluminous alteration rims on chromite grains, in which magmatic cores with cr# ~0.7 and mg# ~0.5, grade into rims with cr# ~0.55 and mg# ~0.6. These are found in highly serpentinised Neoproterozoic chromitites in the Egyptian desert. The alteration is attributed to aluminous, subduction-related fluids. They propose that such metasomatic processes mask primary spinel compositions leading to an incorrect assessment of their former tectonic setting. In this present investigation the samples closest in composition to those described by El-Dien *et al.* (2019) are the Cr–Al spinels from the Oman ophiolite. Our samples do not show the degree of zoning reported by El-Dien, even though there is good evidence for the migration of aluminous felsic melts, related to subduction processes in the Oman ophiolite (Rollinson, 2015). We examined our samples with back-scattered electron imaging (see for example Adetunji *et al.*, 2013; Lenaz *et al.*, 2014) and made

https://doi.org/10.1180/mgm.2023.68 Published online by Cambridge University Press

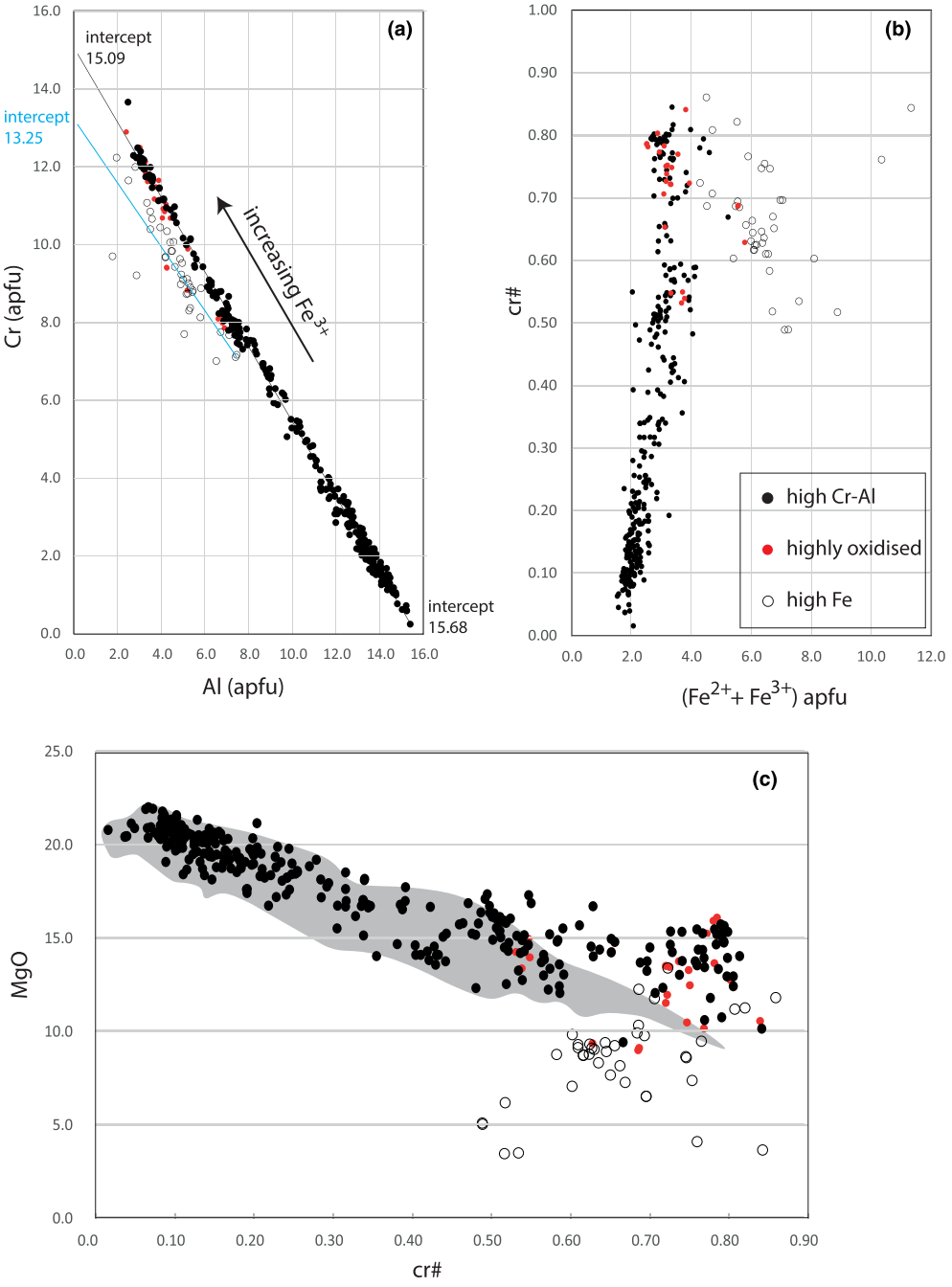

Figure 3. (a) Plot of Al vs. Cr atoms per formula unit (apfu) showing a strong correlation (black circles). A second group of samples (unfilled circles) do not follow this trend but are Cr-poor for a given Al value; the red symbols are samples from the highly oxidised group. The trend lines shown are the best-fit lines together with the relevant intercepts. (b) Plot of (Fe^{3+} + Fe^{2+}) vs. cr# showing the Cr–Al group of samples (black circles), samples that do not conform to this trend (unfilled circles) and the highly oxidised samples (red circles). Samples that do not conform to the Cr–Al correlation have high Fe_{total} and Cr. (c) Plot of MgO vs. cr# for the three groups of spinels shown in (a) and (b). Samples from the Cr–Al group overlap the field identified by Davis et al. (2017) for natural peridotite spinels (n = 743). Samples from the high-Fe group do not conform to this trend. The data in each of these plots are based upon EPMA data corrected with Mössbauer $Fe^{3+}/\Sigma Fe$. The geological setting of the different groups of samples is given in Fig. 1(a and b).

multiple EPMA on each grain and did not find the pattern of reverse zoning described by El-Dien *et al.* (2019). For the most part our samples are not obviously altered and contain fresh olivine. A small number of samples show slight oxidation to ferritchromite on chromite rims and some grains contain small (20–50 mm) silicate and oxide inclusions; even so, average compositions from these samples are within the range of samples without alteration or inclusions. We conclude therefore that our samples have not experienced the metasomatic alteration described by El-Dien *et al.* (2019) and therefore our samples are useful in reflecting the original oxidation state of the parent rocks. The metasomatism described by El-Dien *et al.* (2019) is cryptic. A more persuasive example of metasomatism is found in some anorthositic chromitites where clear replacement textures can be observed (Rollinson *et al.*, 2002).

https://doi.org/10.1180/mgm.2023.68 Published online by Cambridge University Press

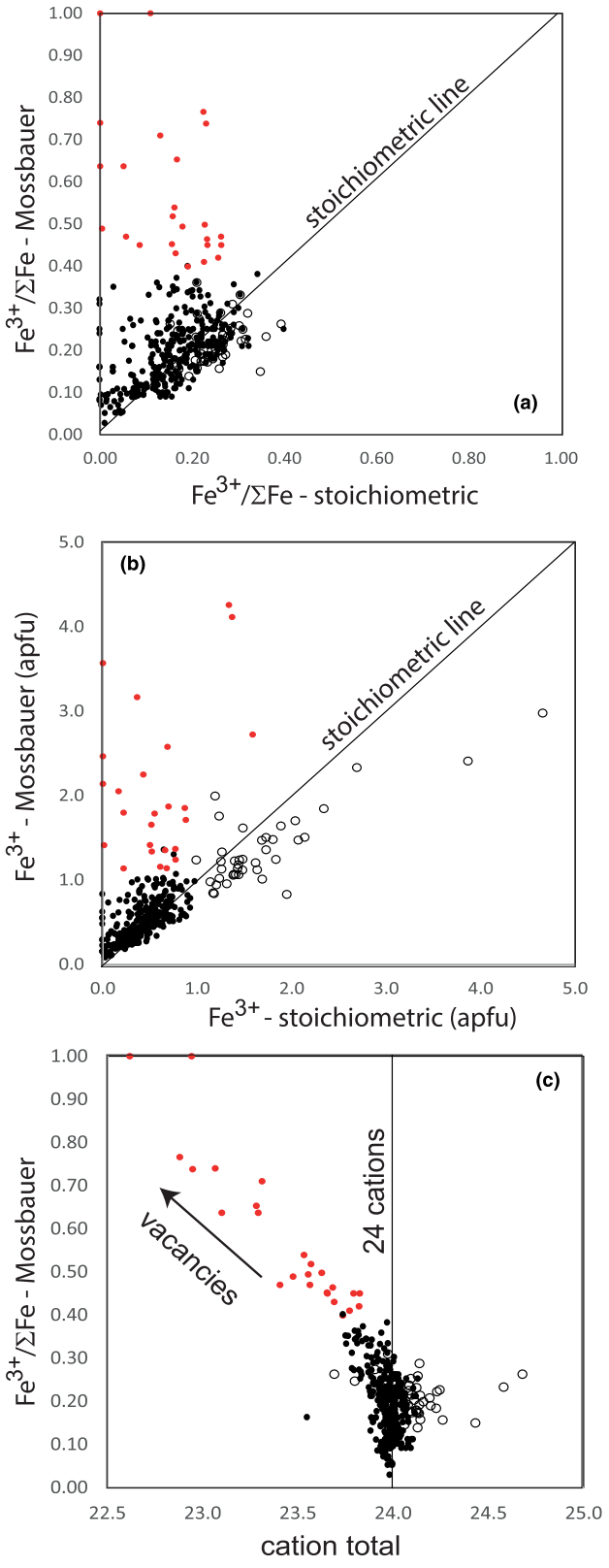

Figure 4. (a) $Fe^{3+}/\Sigma Fe_{Mössbauer}$ vs. $Fe^{3+}/\Sigma Fe_{stoichiometric}$ for the three groups of spinels relative to the stoichiometric line; (b) $Fe^{3+}_{Mössbauer}$ vs. $Fe^{3+}_{stoichiometric}$ as atoms per formula unit (apfu) relative to the 1:1 stoichiometric line; (c) $Fe^{3+}/\Sigma Fe$ vs. cation total relative to the stoichiometric (24.0 cation) line. Symbols as in Figs 1b and 3b. $Fe^{3+}/\Sigma Fe_{Mössbauer}$ means $Fe^{3+}/\Sigma Fe$ as determined by Mössbauer spectroscopy and $Fe^{3+}/\Sigma Fe_{stoichiometric}$ means $Fe^{3+}/\Sigma Fe$ as determined by the Droop (1987) stoichiometric equation. The geological setting of the different sample groups is given in Fig. 1 (a and b).

Highly oxidised spinels

The highly oxidised spinels have $(Fe^{3+}/\Sigma Fe)_{Möss} > 0.4$ (Fig. 2) and high $Fe^{3+}/(Fe^{3+}+Al+Cr)$ ratios in the range 0.16–0.46 (mean = 0.288). However, the $Fe^{3+}/\Sigma Fe$ ratio is significantly underestimated by stoichiometric calculations and these spinels have increasingly low cation totals as Fe^{3+} increases. (Fig. 4a,c). Examination with the scanning electron microscope shows minimal alteration and no evidence that these grains represent a microscopic mixture of phases (Lenaz *et al.*, 2014).

Site-occupancy calculations on a subset of these samples ($n = 7$) reported in Lenaz *et al.* (2014) and plotted in Fig. 5 indicate that the tetrahedrally coordinated site contains Mn and most of the Mg (94–100%) and the octahedrally coordinated site contains all the Cr, Ti, Ni, V and most of the Al (91–100%). Fe^{2+} is distributed between the two sites with 0.0–2.97 apfu on the tetrahedrally coordinated site and 0.0–0.43 on the octahedrally coordinated site; similarly, there are 0.23–2.92 apfu Fe^{3+} on the tetrahedrally coordinated site and 0.16–0.56 apfu on the octahedrally coordinated site. Estimates of vacancies are up to 1.14 apfu on the tetrahedrally coordinated site and up to 0.40 on the octahedrally coordinated site. Though these values are model dependent (see Lenaz *et al.*, 2014 for the details) site-occupancy calculations show that the highly oxidised spinels are characterised by (a) high Fe^{3+} and low Fe^{2+} on the tetrahedrally coordinated site, and (b) low Fe^{3+} and low Fe^{2+} on the octahedrally coordinated site, in addition to higher levels of vacancies on both sites. The low concentration of octahedrally coordinated Fe^{3+} is not consistent with magnetite substitution, but rather implies the oxidation of Fe^{2+} to Fe^{3+} on the tetrahedrally coordinated site as originally proposed by Nell and Pollack (1998).

Where the field relationships have been established for these highly oxidised chromites they are associated with post-magmatic shearing and cataclasis, some of which occurred at high temperature (Lenaz *et al.*, 2014; Adetunji *et al.*, 2013; Figueiras and Waerenborgh, 1997; Menagazzo *et al.*, 1997). The experimental observation of Davis and Cottrell (2018) showed that in a given experiment as f_{O_2} increases, the total abundance of Fe^{3+} increases in the rock-system and Fe^{3+} is preferentially partitioned into spinel at the expense of Cr and Al. This implies a highly oxidising environment for the shearing/ cataclasis indicating either near-surface or hydrous conditions.

The Cr–Al group

The Cr–Al spinel group are characterised by a strong negative correlation on a Cr–Al cation plot ($R^2 = 0.997$). Relative to the other spinel groups they are low in Fe_{total} (Fig. 3b) and have a low $(Fe^{3+}/(Fe^{3+}+Al+Cr)$ ratio (0.007–0.18, mean = 0.055). Most, but not all, samples are stoichiometric (Fig. 4a).

Site occupancy data on a subset of relatively Cr-rich samples ($n = 11$, Lenaz *et al.*, 2014) indicate that all of the Mn and 93–99% of the Mg and 84–100% of the Fe^{2+} are on the tetrahedrally coordinated site and that all of the Cr and 96–100% Al are on the octahedrally coordinated site (Fig. 5). These compositions therefore approximate to normal spinels consistent with the experimental work of Nell *et al.* (1989) and Nell and Wood (1991) in the synthetic systems Fe_3O_4–$FeAl_2O_4$ and Fe_3O_4–$MgCr_2O_4$. The relatively low concentrations of Fe^{3+} are almost equally distributed between the tetrahedrally and octahedrally coordinated sites (0.23–0.66 apfu on the tetrahedrally coordinated site and 0.27–0.80 apfu on the octahedrally coordinated site). This agrees

https://doi.org/10.1180/mgm.2023.68 Published online by Cambridge University Press

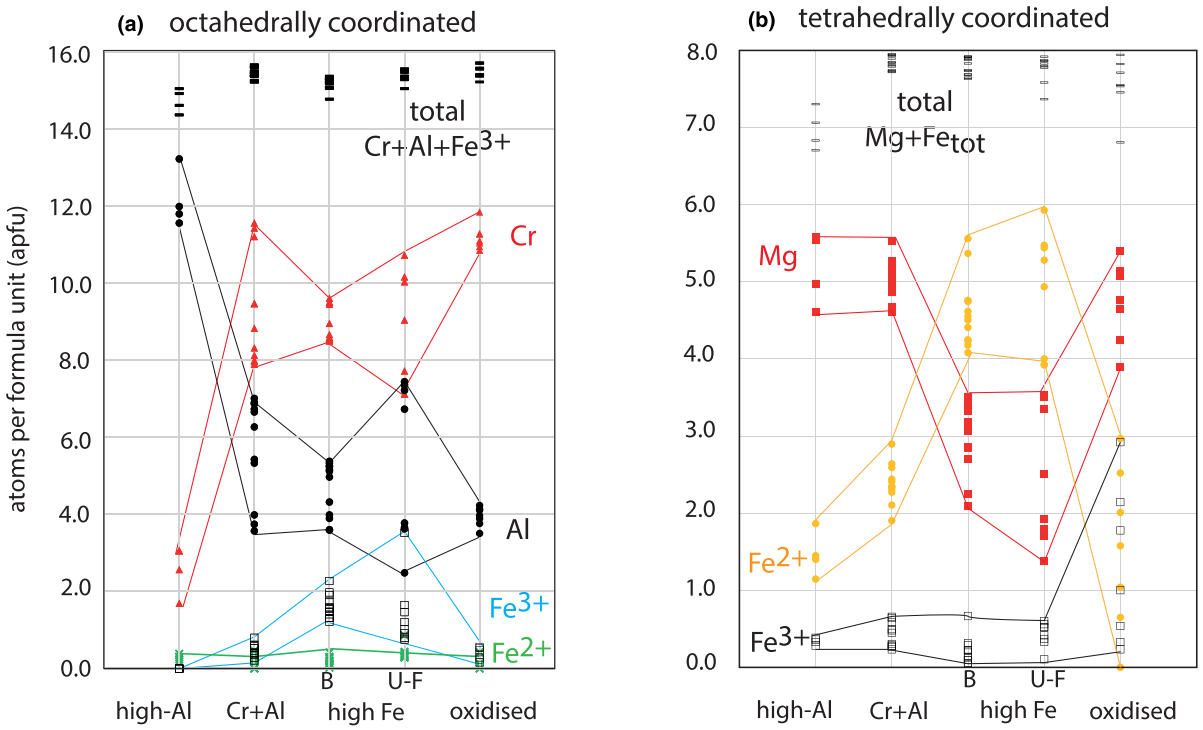

Figure 5. Site occupancies in the high-Al, Cr+Al, high Fe and the highly oxidised spinel groups in atoms per formula unit (apfu). (a) Octahedrally coordinated site occupancies; (b) tetrahedrally coordinated site occupancies. U-F = data from the Ujaragssuit and Fiskenaesset intrusions, B = data from the Bushveld intrusion. Data from Lenaz *et al.* (2007, 2014), Rollinson *et al.* (2017) and Perinelli *et al.* (2012, 2014).

with the Mössbauer studies of Wood and Virgo (1989) and Dyar *et al.* (1989) in natural spinels from spinel lherzolite xenoliths who showed that some Fe^{3+} is tetrahedrally coordinated. In the most aluminous spinels, designated high-Al in Fig. 5, (cr# < 0.2, $n = 4$) 80–89% of the Mg and 83–88% of the Fe^{2+} are on the tetrahedrally coordinated site and 90–95% of the Al is on the octahedrally coordinated site. Fe^{3+} concentrations are very low (0.3–0.4 apfu) and Fe^{3+} is located entirely on the tetrahedrally coordinated site (Fig. 5) (data from Perinelli *et al.*, 2012; 2014).

The high-Fe group

The high-Fe spinels are characterised by Cr > 8.0 apfu, Cr/Cr+Al > 0.49 (Fig. 3a,b) and Fe_{total} > 4.2 apfu (Fig. 3b). They have higher Fe^{3+} than for comparable Cr-rich samples in the Al–Cr group (Fig. 4b) and $Fe^{3+}_{Möss}$ values plot below the stoichiometric line on a $Fe^{3+}_{Möss}$ vs. Fe^{3+}_{stoich} plot (Fig. 4b). In contrast to the Al–Cr spinels they define a weak positive trend on a MgO–cr# plot (Fig. 3c).

We reported site-occupancy data for high-Fe spinels from the Ujaragssuit ($n = 4$) and Fiskenaesset ($n = 4$) intrusions from Greenland in Rollinson *et al.* (2017). In these samples, all the Mn, 84–100% of the Mg and 86–95% of the Fe^{2+} is on the tetrahedrally coordinated site and all of the Ti, Ni and Cr and 90–100% Al are on the octahedrally coordinated site (Fig. 5, column UF). A small amount of Fe^{3+} is present on the tetrahedrally coordinated site (0.10–0.60 apfu) with most on the octahedrally coordinated site (0.75–1.65, one sample 3.5 apfu). There are also data from the Bushveld Complex, which, though not the same samples as reported here, are from the same horizons of the intrusion (n = 12, Lenaz *et al.*, 2007). These data also show that all the Mn, Zn and 83–96% of the Mg and 94–100% of the Fe^{2+} are on the tetrahedrally coordinated site and that all of the Ti, Ni, V and Cr and 94–100% Al are on the octahedrally coordinated site (Fig. 5 column B). A small amount of Fe^{3+} is present on the tetrahedrally coordinated site (0.06–0.60 apfu) with the major portion on the octahedrally coordinated site (1.2–2.3 apfu). In both datasets the site occupancy data indicate that these spinels approximate to normal spinels with most of the Fe^{3+} on the octahedrally coordinated site.

Given that almost all of the Al and all of the Cr are located on the octahedrally coordinated sites in both the Cr–Al spinels and the high-Fe spinels the two trends in Fig. 3a reflect differences in the amount of Fe^{3+} on the octahedrally coordinated site. The Cr–Al spinels contain a small amount of octahedrally coordinated Fe^{3+} (0.27–0.80 apfu, mean = 0.46 apfu) decreasing to zero in the most aluminous samples; in contrast in the high-Fe spinels a greater amount of octahedrally coordinated Fe^{3+} is present (mean = 1.42 apfu in the Ujaragssuit and Fiskenaesset intrusions, mean = 1.62 apfu in the Bushveld).

Recent experimental and thermodynamic studies of peridotite melting by Gaetani, (2016), Sorbadere *et al.* (2018) and Davis and Cottrell (2021) have investigated the partitioning of Fe_2O_3 between spinel and basaltic melt ($D^{spl/melt}_{Fe_2O_3}$). Gaetani (2016) showed that $(Fe^{3+}/\Sigma Fe)_{spin}$ decreases with increasing temperature and pressure although there is some uncertainty about the role of f_{O_2} (Sorbadere *et al.*, 2018). Of significance however, is the observation by Davis and Cottrell (2021) that the partition coefficient increases as a function of the Fe_2O_3 concentration in the spinel, such that Fe_2O_3 is more compatible in the spinels with more Fe. The observation that $D^{spl/melt}_{Fe_2O_3}$ increases as a function of the Fe_2O_3 concentration in spinel is important in this present study because it explains our finding that the high-Fe group of chromites have higher Fe^{3+}. More recently Ajayi *et al.* (2023) have

https://doi.org/10.1180/mgm.2023.68 Published online by Cambridge University Press

reported that the spinel-melt Fe^{3+} partition coefficient also increases with spinel cr#. They show that at a given f_{O_2} $D^{spl/melt}_{Fe_2O_3}$ increases by a factor of ~2 as spinel cr# increases by a factor of ~3.

The observations of Gaetani (2016) and Davis and Cottrell (2021) show that there is an inverse correlation between the partition coefficient $D^{spl/melt}_{Fe_2O_3}$ and temperature; this forms a further control on the partitioning of Fe^{3+} into chromite in cooling mafic intrusions.

Taking together our empirical observations with the experimental data reported above, it is evident that in high Fe–Cr melts available Fe^{3+} is preferentially partitioned into octahedrally coordinated sites in chrome spinels. Our data suggest partitioning occurs where Cr ions occupy more than 50% of the octahedrally coordinated sites so distorting the spinel lattice to accommodate the larger Fe^{3+} octahedrally coordinated ions.

Conclusion: Implications for microprobe correction procedures for Fe^{3+} in spinel

Davis *et al.* (2017) showed recently, in an update of the work of Wood and Virgo (1989), that Fe^{3+} can be accurately measured in spinels by EPMA using a set of secondary microprobe standards in which Fe^{3+} had been determined by Mössbauer spectroscopy. They used the correlation between the offset between $(Fe^{3+}/\Sigma Fe)_{Möss}$ and $(Fe^{3+}/\Sigma Fe)_{EPMA}$ to correct the $Fe^{3+}/\Sigma Fe$ values calculated from EPMA/stoichiometric constraints. Davis *et al.* (2017) recognised that although this correction works well for aluminous spinels in lherzolites it might not be appropriate for spinels outside this compositional range.

Our purpose here has been to place this inference on a sound footing by using data from Cr-rich and Fe-rich spinels in which Fe^{3+} has been accurately determined. Our data show that in addition to the well-known Cr–Al group of spinels there is also a Fe^{3+}–Cr–Al group. Microprobe correction procedures developed for Cr–Al spinels will not apply to spinels from the Fe^{3+}–Cr–Al group as they lie outside the calibration and will lead to errors in calculated Fe^{3+}, as proposed by Davis *et al.* (2017). The distinction between the two spinel groups is also clear on a MgO–cr# plot, where they define two distinct trends, further indicating that spinels of the Fe^{3+}–Cr–Al group are not amenable to the correction procedures relevant to Cr–Al spinels.

For this reason, we urge caution in estimating Fe^{3+} in Cr-bearing spinels determined by EPMA using stoichiometry and in particular samples with high concentrations of Cr and Fe. We suggest a screening method for uncorrected EPMA as follows:

(1) Recalculate the data to cations to 32 oxygens without estimating Fe^{3+};
(2) Sort the data on the basis of (Al+Cr) apfu: samples with (Al +Cr) > ~15.2 belong to the high Cr–Al group; samples with (Al+Cr) < ~15.2 belong to the high Fe group;
(3) This classification can be checked by plotting the data on an Al vs. Cr cation plot: members of the Cr–Al group plot on a trend that intersects the Cr axis at >15.0 apfu; members of the high-Fe group plot below this line and define a trend that intersects the Cr axis at ~13.0 apfu (Fig. S3a);
(4) A further (less precise) check can be made by plotting the data on a cr# vs. fe# diagram: the Cr–Al group plot with fe# <~ 0.5; samples with fe# > 0.5 belong to the high-Fe group (Fig. S3b).

Stoichiometric estimates of Fe^{3+} for uncorrected EPMA data for the Cr–Al spinels are close to the true values as determined by Mössbauer, although we would recommend that if accurate $Fe^{3+}/\Sigma Fe$ ratios are required for f_{O_2} calculations then the Wood and Virgo (1989) / Davis *et al.* (2017) correction must also be applied. Our data do not confirm the correction procedure proposed by Langa *et al.* (2021) for Fe-rich spinels. Finally, it is important to note that samples in the highly oxidised group are very difficult to identify without Mössbauer spectroscopy. However, field evidence of high-temperature shearing and/or petrographic evidence of cataclasis should alert the user (see Adetunji *et al.*, 2013). Recognising them is important, for misidentification can lead to errors in Fe^{3+}, and resultant errors in $Fe^{3+}/\Sigma Fe$ as great as 0.2–0.5 (Fig. 4a).

Acknowledgements. We thank Rohaiza bint Zachariah (Sultan Qaboos University), Ben Sutherland, Dona John, Callum Prescott and Georgia Pulford (all from the University of Derby) for their assistance in the many days of preparation and hand picking of pure chromite concentrates for Mössbauer spectroscopy and Stuart Kearnes (University of Bristol) and Graham Souch (University of Derby) for help with the analytical work. This study was supported by grant IG/SCI/ETHS/ 04/02 from the Research Committee of the College of Science, Sultan Qaboos University, Oman, RLTF 2011 and 2012 grants from the University of Derby and an award from the Nuffield Foundation Science Bursary scheme. Samples from Ujaragssuit and Seqi were collected in association with the Greenland Geological Survey; the Fiskenaesset samples were provided by Brian Windley. We thank Duncan Jarman for the Brakfontein (Bushveld) drill core. We are very grateful to Suzanne Birner, Vincenzo Stagno and several anonymous reviewers for their helpful comments on earlier versions of this manuscript that have led to substantial improvements.

Supplementary material. The supplementary material for this article can be found at https://doi.org/10.1180/mgm.2023.68.

Competing interests. The authors declare none.

References

Adetunji J., Everitt S. and Rollinson H. (2013) New Mössbauer measurements of $Fe^{3+}/\Sigma Fe$ ratios in chromites from the early Proterozoic Bushveld Complex, South Africa. *Precambrian Research*, **228**, 194–205.

Ajayi A.R., Davis F. and Cottrell, E. (2023) Spinel-melt Fe^{3+} partition coefficient increases with spinel cr#. *Goldschmidt conference abstracts*, https://conf.goldschmidt.info/goldschmidt/2023/meetingapp.cgi/Paper/19954

Arai S. (1994) Characterisation of spinel peridotites by olivine-spinel compositional relationships: review and interpretation. *Chemical Geology*, **113**, 191–204.

Ballhaus C., Berry R.F. and Green D.H. (1991) High pressure experimental calibration of the olivine-orthopyroxene-spinel oxygen geobarometer: implications for the oxidation state of the upper mantle. *Contributions to Mineralogy and Petrology*, **107**, 27–40.

Bosi F., Andreozzi G.B., Ferrini V. and Lucchesi S. (2004) Behaviour of cation vacancy in kenotetrahedral Cr-spinels from Albanian eastern belt ophiolites. *American Mineralogist*, **89**, 1367–73.

Bosi F., Biagioni C. and Pasero M. (2019) Nomenclature and classification of the spinel supergroup. *European Journal of Mineralogy*, **31**, 183–192.

Canil D., Virgo D. and Scarfe C.M. (1990) Oxidation state of mantle xenoliths from British Columbia, Canada. *Contributions to Mineralogy and Petrology*, **104**, 453–462.

Dare S.A.S., Pearce J.A., McDonald I. and Styles M.T. (2009) Tectonic discrimination of peridotites using f_{O_2}–Cr# and Ga–Ti–FeIII systematics in chrome–spinel. *Chemical Geology*, **261**, 199–216

Davis F.A. and Cottrell E. (2018) Experimental investigation of basalt and peridotite oxybarometers: implications for spinel thermodynamic models and Fe^{3+} compatibility during generation of upper mantle melts. *American Mineralogist*, **103**, 1056–1067.

Davis F.A. and Cottrell E. (2021) Partitioning of Fe_2O_3 in peridotite partial melting experiments over a range of oxygen fugacities elucidates ferric iron systematics in mid-ocean ridge basalts and ferric iron content of the upper mantle. *Contributions to Mineralogy and Petrology*, **176**, 67.

Davis F.A., Cottrell E., Birner S.K., Warren J.M. and Lopez O.G. (2017) Revisiting the electron microprobe method of spinel-olivine-orthopyroxene oxybarometry applied to spinel peridotites. *American Mineralogist*, **102**, 421–435.

Droop G.T.R. (1987) A general equation for estimating Fe^{3+} concentrations in ferromagnesian silicates and oxides from microprobe analyses, using stoichiometric criteria. *Mineralogical Magazine*, **51**, 431–435.

Dyar M.D., McGuire A.V. and Ziegler R.D. (1989) Redox equilibria and crystal chemistry of coexisting minerals from spinel lherzolite mantle xenoliths. *American Mineralogist*, **74**, 969–980.

El-Dien H.G., Arai S., Doucet L-S., Li Z-X., Kil Y., Fougerouse D., Reddy S.M., Saxey D.W. and Hamdy M. (2019) Cr-spinel records metasomatism not petrogenesis of mantle rocks. *Nature Communications*, **10**, 5103.

Figueiras J. and Waerenborgh J.C. (1997) Fully oxidized chromite in the Serra Alta (South Portugal) quartzites: chemical and structural characterization and geological implications. *Mineralogical Magazine*, **61**, 627–638.

Fregola R.A., Bosi F. and Skogby H. (2011) A first report on anion vacancies in a defect $MgAl_2O_4$ natural spinel. *Periodico di Mineralogia*, **80**, 27–38.

Gaetani G.A. (2016) The behavior of $Fe^{3+}/\Sigma Fe$ during partial melting of spinel lherzolite. *Geochimica Cosmochimica Acta*, **185**, 64–77.

Haggerty S.E. (1991) Oxide mineralogy of the upper mantle. Pp. 355–416 in: *Oxide Minerals: Petrologic and Magnetic Significance* (D.H. Lindsley, editor). Reviews in Mineralogy, **25**. Mineralogical Society of America, Washington D.C.

Langa M.M., Jugo P., Leybourne M.I., Grobler D.F., Adetunji J. and Skogby H. (2021) Chromite chemistry of a massive chromitite seam in the northern limb of the Bushveld Igneous Complex, South Africa: Correlation with the UG-2 in the eastern and western limbs and evidence of variable assimilation of footwall rocks. *Mineralium Deposita*, **56**, 31–44.

Lenaz D., Braidotti R., Princivalle F., Garuti G. and Zaccarini F. (2007) Crystal chemistry and structural refinement of chromites from different layers and xenoliths in the Bushveld Complex. *European Journal of Mineralogy*, **19**, 599–609.

Lenaz D., O'Driscoll B. and Princivalle F. (2011) Petrogenesis of the anorthosite-chromitite association: crystal-chemical and petrological insights from the Rum Layered Suite, NW Scotland. *Contributions to Mineralogy and Petrology*, **162**, 1201–1213.

Lenaz D., Adetunji J. and Rollinson H. (2014) Determination of $Fe^{3+}/\Sigma Fe$ ratios in chrome spinels using a combined Mossbauer and single-crystal X-ray approach: application to chromitites from the mantle section of the Oman ophiolite. *Contributions to Mineralogy and Petrology*, **167**, 958.

Menagazzo G., Carbonin S. and Della Giusta A. (1997) Cation and vacancy distribution in an artificially oxidized natural spinel. *Mineralogical Magazine*, **61**, 441–421.

Nell J. and Pollack H. (1998) Cation to anion stoichiometry of chromite: A new perspective. *Hyperfine interactions*, **111**, 309–312.

Nell J. and Wood B.J. (1989) Thermodynamic properties in a multicomponent component solid solution involving cation disorder: Fe_3O_4–$MgFe_2O_4$–$FeAl_2O_4$–$MgAl_2O_4$ spinels. *American Mineralogist*, **74**, 1000–1015.

Nell J. and Wood B.J. (1991) High-temperature electrical measurements and thermodynamic properties of Fe_3O_4–$FeCr_2O_4$–$MgCr_2O_4$–$FeAl_2O_4$ spinels. *American Mineralogist*, **76**, 405–426.

Nell J., Wood B.J. and Mason T.O. (1989) High-temperature cation distributions in Fe_3O_4–$MgFe_2O_4$–$FeAl_2O_4$–$MgAl_2O_4$ spinels from thermopower and conductivity measurements. *American Mineralogist*, **74**, 339–354.

O'Driscoll B., Leuthold J., Lenaz D., Skogby H., Day J.M. and Adetunji J. (2021) Melt percolation, melt-rock reaction and oxygen fugacity in suprasubduction zone mantle and lower crust from the Leka Ophiolite Complex, Norway. *Journal of Petrology*, **62**, 1–26.

O'Neill H. St C. and Navrotsky A. (1983) Simple spinels: crystallographic parameters, cation radii, lattice energies, and cation distribution. *American Mineralogist*, **68**, 181–194.

Perinelli C., Andreozzi G.B., Conte A.M. and Armienti P. (2014) Geothermometric study of Cr-spinels of peridotite mantle xenoliths from northern Victoria Land (Antarctica). *American Mineralogist*, **99**, 839–846.

Perinelli C., Bosi F., Andreozzi G.B., Conte A.M., Oberti R. and Armienti P. (2012) Redox state of subcontinental lithospheric mantle and relationships with metasomatism: insights from spinel peridotites from northern Victoria Land (Antarctica). *Contributions to Mineralogy and Petrology*, **164**, 1053–1067.

Rollinson H.R. (2015) Slab and sediment melting during subduction initiation: Granitoid dykes from the mantle section of the Oman ophiolite: *Contributions to Mineralogy and Petrology*, **170**, 32–52.

Rollinson H.R. and Adetunji J. (2013) Mantle podiform chromitites do not form beneath mid-ocean ridges: A case study from the Moho transition zone of the Oman ophiolite. *Lithos*, **177**, 314–327.

Rollinson H.R., Appel P.W.U. and Frei R. (2002) A metamorphosed, Early Archean chromitite from West Greenland: implications for the genesis of Archaean anorthositic chromitites. *Journal of Petrology*, **43**, 2143–2170.

Rollinson H.R., Adetunji J., Yousif A.A. and Gismelseed A.M. (2012) New Mossbauer measurements of $Fe^{3+}/\Sigma Fe$ in chromites from the mantle section of the Oman ophiolite: evidence for the oxidation of the sub-oceanic mantle. *Mineralogical Magazine*, **76**, 579–596.

Rollinson H.R., Adetunji J., Lenaz D. and Szilas K. (2017) Archaean chromitites show constant $Fe^{3+}/\Sigma Fe$ in Earth's asthenospheric mantle since 3.8 Ga. *Lithos*, **282–283**, 316–325.

Schmidbauer E. (1987) Fe–57 Mössbauer-spectroscopy and magnetization of cation deficient Fe_2TiO_4 and $FeCr_2O_4$ 2. Magnetization data. *Physics and Chemistry of Minerals*, **15**, 201–207.

Sorbadere F., Laurenz V., Frost D.J., Wenz M., Rosenthal A., McCammon C. and Rivard C. (2018) The behaviour of ferric iron during partial melting of peridotite *Geochimica Cosmochimica Acta*, **239**, 235–254.

Stagno V. (2019) Carbon, carbides and carbonatitic melts in the Earth's interior. *Journal of the Geological Society*, **176**, 375–387.

Stagno V. and Fei Y. (2020) The redox boundaries of Earth's interior. *Elements*, **16**, 167–172.

Velicogna M. and Lenaz D. (2017) Is 600 °C enough to produce air oxidation in Cr-spinels? *Neues Jahrbuch für Mineralogie* (*Journal of Mineralogy and* Geochemistry), **194**/2, 125–137.

Wood B.J. (1990) An experimental test of the spinel peridotite oxygen barometer. *Journal of Geophysical Research*, **95B**, 15845–15851.

Wood B.J. and Virgo D. (1989) Upper mantle oxidation state: ferric iron contents of lherzolite spinels by ^{57}Fe Mössbauer spectroscopy and resultant oxygen fugacities. *Geochimica et Cosmochimica Acta*, **53**, 1277–1291.

https://doi.org/10.1180/mgm.2023.68 Published online by Cambridge University Press